BULLETIN OF THE POLISH ACADEMY OF SCIENCES
TECHNICAL SCIENCES, Vol. 74(3), 2026, Article number: e158300
DOI: 10.24425/bpasts.2026.158300

The role of YRNA-derived small RNAs in atherosclerosis development and progression – modeled and analyzed using Petri nets

Adam TRZEBIATOWSKI[1] and **Agnieszka RYBARCZYK**[1,2]*

[1] Faculty of Electrical Engineering, Gdynia Maritime University, 81-225 Gdynia, Poland
[2] Institute of Computing Science, Poznan University of Technology, 60-965 Poznan, Poland

Abstract. Non-coding RNAs regulate diverse aspects of development, homeostasis, and disease. Among them, YRNA–derived small RNAs (s-RNYs) have attracted clinical interest as potential biomarkers due to their high abundance across human tissues, body fluids, and tumors. Despite major advances in understanding atherogenesis, the overall picture remains incomplete, limiting therapeutic progress. To address this gap, we built a systems model of atherogenesis using classical Petri nets, integrating recent insights of s-RNY functions in monocytes and macrophages alongside oxidative stress, inflammatory signaling, and key atherogenic pathways. Using t-invariant analysis, in silico knockouts, and dynamic simulations, we found that dual-target strategies, such as suppression of oxidative stress combined with inhibition of either (1) toll-like receptor 7 (TLR7), (2) s-RNYs, or (3) the pro-inflammatory cytokine interleukin-6 (IL-6), attenuate lesion progression. These findings support multi-pathway combination therapy as a promising direction to more effective treatment of atherosclerosis.

Keywords: small RNAs; atherosclerosis; systems biology; Petri nets; t-invariants.

1. INTRODUCTION

Despite great progress in understanding the pathomechanisms underlying atherosclerosis, our knowledge of this condition remains incomplete, making it difficult to develop effective treatments. Atherosclerosis is a chronic systemic inflammatory disease of the arteries, characterized by the formation of lipid-rich atherosclerotic plaques in the inner layer of their walls. The inflammatory process within blood vessels leads to the development of unstable atherosclerotic lesions, which, over time, can restrict blood flow, impairing the blood supply to tissues and organs. Numerous cells of the immune system are involved in the formation of atherosclerotic plaques, as well as growth factors and pro-inflammatory mediators [1–3]. Together, these interactions shape characteristic molecular signatures that can be systematically profiled.

Atherosclerosis can be assessed at multiple molecular levels, including proteomic, lipidomic, transcriptomic (RNA), and genomic analyses [4, 5]. Within the RNA domain, the discovery and use of non-coding RNAs enclosed in extracellular vesicles (EVs, exosomes) show promise for novel diagnostic and therapeutic applications [4, 6–8].

Exosomes are 40–100 nm spherical lipid bilayer extracellular vesicles released by many types of eukaryotic cells under physiological and pathological conditions. Formed by inward budding into multivesicular bodies and released after fusion with the plasma membrane, exosomes carry proteins, lipids, and diverse RNAs. Exosomes have recently attracted growing interest due to their great potential for drug delivery [9]. They can be selectively taken up by nearby or distant recipient cells, where their cargo modulates gene expression and cellular function, allowing paracrine exchange of molecular signals [10–12]. Among this cargo, non-coding RNAs (ncRNAs) are of particular interest.

Non-coding RNAs are classified by transcript length. Small noncoding RNAs (sncRNAs) have fewer than 200 nucleotides (nt), while long noncoding RNAs (lncRNAs) exceed 200 nt. Small RNAs are actively profiled with next-generation sequencing to identify circulating and EV-associated signatures, as well as tissue context signals within atherosclerotic plaques [13, 14]. Contemporary workflows span EV enrichment, small-RNA library preparation, and targeted validation [15]. Among small-RNA classes, YRNAs are a class of small non-coding RNAs (sncRNAs) that have attracted growing interest. Their circulating fragments (YsRNAs) are likely generated by ribonuclease 1 (RNase 1) [16]. The mechanisms by which extracellular vesicles (EVs) export YRNAs to the extracellular space have been thoroughly reviewed [5, 6]. Recent studies show that EV-associated YRNAs contribute to the initiation and progression of atherosclerosis and may aid in diagnosis [5, 6, 17–19]. The increased 5′- and 3′-derived YRNA fragments were reported in sera from patients with atherosclerosis by [17]. Beyond atherosclerosis, circulating YRNA fragments have been explored as minimally invasive biomarkers in breast cancer [20] and squamous cell carcinoma [21], and have been proposed as diagnostic and prognostic markers in coronary artery disease [17].

*e-mail: a.rybarczyk@we.umg.edu.pl

Manuscript submitted 2025-09-15, revised 2026-02-20, initially accepted for publication 2026-02-23, published in May 2026.

Functionally, YRNAs interact with multiple proteins implicated in atherogenesis, including nucleolin, Z-DNA binding protein 1 (ZBP1), YRNA binding protein (Ro60) and 52 kDa ribonucleoprotein (Ro52), poly(U) binding splicing factor 60 (PUF60, RoBPI), large subunit ribosomal protein 5 (RPL5, L5), human Sjogren syndrome antigen B (La/SSB), heterogeneous nuclear ribonucleoprotein K (hnRNP-K), and heterogeneous nuclear ribonucleoprotein I (hnRNPI) [5]. Ro60 is pivotal for YRNA fragment-mediated apoptosis and inflammation [7, 18], and anti-Ro antibodies, often accompanied by anti-La, are strongly associated with anti-oxidized-low-density lipoprotein (anti-ox-LDL) or anti-phospholipid antibodies [8]. Moreover, recent studies indicate that small regulatory RNAs (s-RNAs), formed from YRNAs, can act as independent biomarkers of coronary artery changes associated with the progression of atherosclerosis [6, 17, 18]. In the presence of atherogenic factors, such as oxidized low-density-lipoprotein (ox-LDL), s-RNA/Ro60 complexes are formed in macrophages from RNA molecules that activate the toll-like receptor 7 (TLR7). This leads to the activation of signaling pathways dependent on nuclear factor kappa light chain enhancer of activated B cells (NF-κB), a key transcription factor that induces the production of pro-inflammatory cytokines, and the activation of caspase-3 and the initiation of apoptosis [3, 17, 22].

As a result of macrophage death, s-RNA/Ro60 complexes spread, increasing inflammation and further apoptosis, which may contribute to the progression of atherosclerotic lesions. In addition, TLR7 activation increases ox-LDL uptake by macrophages and the production of reactive oxygen species, enhancing low-density lipoprotein (LDL) oxidation, fueling a vicious cycle of inflammation and accelerating the development of atherosclerosis [17, 22].

Given the multifactorial nature of atherosclerosis, no single biomarker currently provides a definitive assessment of disease severity or reliably predicts cardiovascular risk [23]. Consequently, ongoing efforts are aimed at indicating key pathways to improve understanding and therapeutic strategies. To our knowledge, this is the first study to integrate, within a single framework, many signaling pathways and core processes that link YRNA-derived small RNA (sRNA) to the regulation of apoptosis and inflammation in monocytes/macrophages, together with mechanisms driving atherosclerosis. This integration employs the Petri net theory, which enables the construction of molecular interaction networks without precise quantitative parameters, in contrast to ordinary and partial differential equation (ODE/PDE) approaches that require well-specified rate constants [24]. The limited availability of reliable quantitative reaction data often constrains the ODE/PDE modeling, particularly for complex biological systems [25].

Despite a rapidly expanding experimental and biomarker literature on non-coding RNAs in atherosclerosis, integrative mathematical models that explicitly account for RNA-mediated regulation remain scarce. Contemporary atherogenesis frameworks, ODE/PDE formulations, continuum mechanics, and agent-based models primarily capture lipids, hemodynamics, and inflammation [26–29]. On the other hand, RNA-centric studies are predominantly statistical or biomarker-driven [13–15, 30, 31].

In this study, we used classical Petri nets to investigate mechanisms that recent evidence suggests are central to atherosclerosis [3, 24]. We first built a model integrating emerging findings—most notably the roles of YRNA–derived small RNAs (s-RNYs) in monocytes and macrophages, together with oxidative stress, inflammatory signaling, and the principal pathways driving atherogenesis. To assess the contribution of individual components, we performed in silico knockouts, removing selected nodes and evaluating system behavior in their absence. This approach enabled us to rank the relative importance of these factors.

2. METHODOLOGY

2.1. Petri nets

A Petri net is a mathematical object with the structure of a directed bipartite graph, which means that its set of vertices can be divided into two disjoint subsets in such a way that each arc only connects vertices belonging to different subsets. In a Petri net, vertices belonging to one of the mentioned subsets are referred to as places, and those belonging to the other are called transitions [32]. In the context of biological systems, transitions correspond to elementary processes, and places represent the components necessary for their occurrence or resulting from them.

However, a bipartite graph alone is not sufficient to represent the behavior of a system, while the ability to model its dynamics is one of the key properties of Petri nets. For this, one needs tokens located in places that reflect the quantitative states of the system's components. Their distribution, or so-called marking, describes the current state of the modeled system (since the number of tokens located at a given place represents the amount of a specific, passive component of the system present in it at a given moment and represented by that place).

Tokens move in the Petri net between places via transitions, according to the activation rule. A transition becomes active when all of its input places have a number of tokens not less than the weight of the assigned arc. When a transition is activated, tokens are removed from the input places and added to the output places, according to the weights of the arcs.

Besides the graphical representation of the Petri net, which is transparent and intuitive to humans, its structure (directed bipartite graph) can also be represented using an incidence matrix (neighborhood matrix). This matrix, denoted $C = [c_{ij}]_{nxm}$, consists of n rows and m columns, and each of its elements c_{ij} represents the change in the number of tokens at place p_i after the initiation of a transition t_j [32]. Transition invariants (t-invariants) can be determined from the C matrix, and are the basis for most structural analyses of the network. An invariant is a vector x, which satisfies the equation $C \bullet x = 0$. Associated with the invariant x is a set of transitions $supp(x) = \{t_j : x_j > 0\}$ called its support. It includes all transitions for which the corresponding positions in the vector x have values greater than zero. If all the transitions from the support of a given t-invariant are activated (in the order implied by the network structure), then the state of the network will not change. From a biological point of view, a t-invariant (its support) defines a certain subset of

reactions for which the overall execution does not disturb the balance of the biological system [32, 33].

The analysis of t-invariants plays an important role in modeling complex biological systems, since they correspond to certain subprocesses in the system under study. Some of these subprocesses may interact with each other, which is reflected in the structure of the set of t-invariants. The search for such connections makes it possible to identify new, previously unknown characteristics of the system under study [24].

Such analyses can be carried out on the basis of two structures: MCT sets (maximum common transitions sets) and t-clusters [34]. The first of these, MCT sets, represent the division of a set of transitions into disjoint subsets, each of which corresponds to a certain functional module (block) of the system under study. Each of the MCT sets contains transitions that are elements of supports of exactly the same t-invariants.

Apart from grouping transitions into MCT-sets, t-invariants can also be organised into t-clusters. This is motivated by the fact that similar t-invariants correspond to transition sets (i.e., their supports) that overlap, meaning their intersections are non-empty. Consequently, such invariants can be viewed as counterparts of subprocesses that share some elementary subprocesses. These elementary subprocesses correspond to transitions belonging to the intersections of the supports. Through these common elementary subprocesses, the corresponding subprocesses may interact. Therefore, identifying similarities among t-invariants can reveal previously unknown system properties arising from such interactions.

From a biological perspective, t-invariants are particularly interesting because they represent reproducible subprocesses occurring in the modelled system. In complex models, the number of t-invariants is often large, which makes direct similarity analysis difficult. For this reason, common properties and similarities between t-invariants are typically investigated using standard clustering methods. T-invariants can then be grouped into sets called t-clusters, where each cluster contains t-invariants that are similar according to a chosen similarity measure [35]. While clustering alone is usually not sufficient to fully identify all meaningful similarities between subprocesses, it indicates where such similarities are most likely to be found, namely, within the identified t-clusters.

Choosing a meaningful clustering requires selecting an appropriate clustering algorithm, a suitable similarity measure, and the number of clusters. In general, there are no universal rules for making these choices, so they must be made carefully and in the context of the analysed system. One practical approach is to generate multiple alternative clusterings and then assess their quality using indices such as mean split silhouette (MSS) and the Calinski–Harabasz (C–H) index [36–39]. A similarity of two t-invariants can, for example, be quantified using the Pearson correlation coefficient, which reflects the overlap of transitions occurring in the supports of both t-invariants by determining the collinearity of their vectors in an n-dimensional space. By analysing the properties of t-invariants within a cluster, one can assign a biological meaning to the cluster, identify interactions between subprocesses represented by similar t-invariants, and draw biological conclusions [33, 40].

In our study, we used the MSS index to select the best clustering and, in particular, to determine the optimal number of t-clusters [41]. Building on prior analyses in which multiple candidate clusterings were compared across different methodological choices [39, 41], we based further investigations on clusters obtained with the unweighted pair group method with arithmetic mean (UPGMA) agglomeration procedure combined with Pearson-correlation–based similarity, an approach reported to yield robust results in t-cluster analyses of Petri net models [35, 39, 41].

Petri net models of biological systems can also be analyzed by disabling selected parts of the network and observing the resulting behavior, a method known as knockout analysis [24]. Two approaches can be distinguished: (i) t-invariant–based analysis, where disabling specific transitions eliminates certain t-invariants, revealing affected subprocesses; and (ii) simulation-based analysis, where transitions are disabled and the resulting token distributions are examined across multiple runs with identical initial conditions. Both approaches assess the impact of individual or grouped transitions on system behavior.

2.2. Biological background

This subsection presents the modeled phenomena together with their detailed characteristics, as well as the corresponding place and transition symbols included in the model. Each place and transition is denoted by p_x and t_y, respectively, where x and y refer to their numbers listed in Tables 1 and 2.

Atherosclerosis is a chronic systemic inflammatory disease of the arteries, characterized by the formation of plaques rich in lipids within the intima. In the early stages, deposits of macrophages p_{27}, low-density lipoproteins (LDL; p_{42}, t_{55}), foam cells (p_{28}, p_{31}, t_{32}, t_{54}), and extracellular cholesterol accumulate, forming fatty streaks, the earliest atherosclerotic lesions. Over time, these evolve into advanced luminal-narrowing lesions (p_{29}, t_{34}), enriched with fibrous connective tissue that encapsulates the inflammatory core [3, 46]. A key factor in disease progression is the modification of LDL (p_{42}, t_3, t_{55}), mainly through oxidation, producing ox-LDL (p_3, t_3). Modified lipoproteins trigger endothelial inflammation (p_{21}, p_{34}, t_{23}, t_{39}), leading to adhesion molecule expression (p_{25}, t_{30}, t_{48}), leukocyte recruitment, and monocyte migration (p_{26}, t_{31}). These differentiate into macrophages (p_{27}, t_{32}) expressing scavenger receptors (p_{40}, t_{51}) [3]. Inflammation promotes the development of unstable plaques with thin fibrous caps (p_{40}, t_{47}), abundant inflammatory cells (t_{39}), and large lipid cores, which are closely associated with increased vulnerability and a high risk of rupture followed by thrombosis (p_{37}, t_{47}) [3, 46].

Recent studies have demonstrated that small regulatory RNAs (s-RNY), derived from YRNAs (p_0–p_2, t_0–t_2, t_4, t_5), can serve as biomarkers of coronary artery disease and are associated with atherosclerotic lesion progression (t_{35}). Under atherogenic stimuli such as ox-LDL (p_3, t_3), macrophages produce s-RNY forming complexes with Ro60 (p_4, t_2, t_6). These complexes activate TLR7 (p_6, t_6), triggering NF-κB–dependent signaling (p_7–p_{19}, t_9–t_{22}) and apoptosis (p_{43}, t_{24}) via caspase-3 (p_{20}, t_{25}) [42].

Table 1
The list of network places and their biological meaning

Place	Biological meaning	References	Place	Biological meaning	References
p_0	YRNA	[42]	p_{22}	reactive oxygen and nitrogen species	[17,43,44]
p_1	Ro60	[42]	p_{23}	iNOS (inducible nitric oxide synthase)	[3,17,22]
p_2	YRNA Ro60 complex (Ro ribonucleoprotein particle, RoRNP)	[42]	p_{24}	nitrogen oxide NO	[17,43,44]
p_3	ox-LDL	[3,17,42–45]	p_{25}	adhesion molecules ICAM1 (intercellular adhesion molecule-1) VCAM1 (vascular cell adhesion molecule-1)	[3,17,22,42]
p_4	sRNY Ro60 complex	[17,42]	p_{26}	monocytes in the subendothelial intima	[3,45]
p_5	extracellular sRNY Ro60	[17]	p_{27}	macrophages in the subendothelial intima	[3,17,46]
p_6	activated TLR7	[3,17,22,42,47]	p_{28}	foam cells	[3,17,46]
p_7	TLR7 MyD88 (myeloid differentiation primary response 88) complex	[3,17,22,42]	p_{29}	atherosclerotic plaque	[3,46]
p_8	TLR7 MyD88 IRAK4 (interleukin-1 receptor-associated kinase 4) complex	[3,17,22,42]	p_{30}	MCP1 (monocyte chemoattractant protein-1)	[3,17,22,45]
p_9	TLR7 MyD88 IRAK4 IRAK1 (interleukin-1 receptor-associated kinase 1) complex	[3,17,22,42]	p_{31}	activated macrophages loaded with ox-LDL	[3,46]
p_{10}	TLR7 MyD88 IRAK4 IRAK1 1P (phosphorylated) complex	[3,17,22,42]	p_{32}	IL-6R (interleukin-6 receptor) IL-6 JAK (Janus kinase) complex	[3,46,48]
p_{11}	TLR7 MyD88 IRAK4 IRAK1 1P TRAF6 (tumor necrosis factor receptor–associated factor 6) complex	[3,17,22,42]	p_{33}	JAK kinase	[48]
p_{12}	TLR7 MyD88 TRAF6 complex	[3,17,22,42]	p_{34}	IL-6	[3,17,22,45,48,49]
p_{13}	active IKK (inhibitor of nuclear factor kappa-B kinase) complex	[3,17,22,42]	p_{35}	IL-6R IL-6 complex	[48]
p_{14}	phosphorylated I-κB (inhibitor of NF-κB) (I-κB NF-κB complex)	[3,17,22,42]	p_{36}	IL-6R	[48]
p_{15}	I-κB P (phosphorylated inhibitor of NF-κB)	[3,17,22,42]	p_{37}	atherosclerotic plaque rupture	[3,46]
p_{16}	NF-κB cytoplasm	[3,17,22,42]	p_{38}	STAT3 (signal transducer and activator of transcription 3) translocation into the nucleus	[48]
p_{17}	NF-κB in the nucleus	[3,17,22,42]	p_{39}	active MAPK (mitogen-activated protein kinase) kinase	[48]
p_{18}	I-κB NF-κB complex	[3,17,22,42]	p_{40}	macrophages with scavenger receptors	[3,45,46]
p_{19}	I-κB	[3,17,22,42]	p_{41}	NADPH oxidase (nicotinamide adenine dinucleotide phosphate oxidase)	[3,17,43,44,46]
p_{20}	active caspase 3	[42]	p_{42}	LDL	[3,46]
p_{21}	TNF (tumor necrosis factor)	[3,17,22,45,49]	p_{43}	apoptotic body	[17,42]

Within the NF-κB–dependent signaling pathway (p_7–p_{19}, t_9–t_{22}), activation of TLR7 (p_6, t_6) recruits the myeloid differentiation primary response 88 (MyD88) protein (p_7, t_9), which initiates interleukin-1 receptor-associated kinase 4 (IRAK-4) recruitment (p_8, t_{10}). IRAK-4 phosphorylates interleukin-1 receptor-associated kinase 1 (IRAK-1) (p_9, p_{10}, t_{11}, t_{12}), allowing binding of tumor necrosis factor receptor–associated factor 6 (TRAF6) (p_{11}, t_{13}). Following phosphorylation, these kinases dissociate from MyD88 (t_{14}), and the resulting complex stimulates the phosphorylation of inhibitor of NF-κB (I-κB) bound to NF-κB (p_{12}, p_{13}, p_{14}, t_{14}–t_{16}) [3,17,22,47].

NF-κB dimers normally remain in the cytoplasm in an inactive state, bound to their inhibitor I-κB (p_{18}, t_{22}). Upon kinase activation, I-κB undergoes dissociation, ubiquitination, and subsequent degradation (p_{15}, t_{17}, t_{18}). Freed NF-κB dimers are then translocated into the nucleus (p_{16}, p_{17}, t_{19}), where they bind DNA and induce expression of pro-inflammatory genes, including tumor necrosis factor alpha (TNF-α) (p_{21}, t_{23}), interleukin-6

Table 2
The list of network transitions and their biological meaning

Transition	Biological meaning	References	Transition	Biological meaning	References
t_0	transcription of YRNA genes by Polymerase III	[42]	t_{29}	cardiovascular failure	[43–45, 49]
t_1	YRNA Ro60 binding	[42]	t_{30}	expression of adhesion molecules ICAM1 VCAM1	[3, 17, 22]
t_2	degradation of YRNA to sRNA	[42]	t_{31}	recruitment and the process of adhesion of monocytes to the endothelium	[3]
t_3	lipids peroxidation	[3, 17, 43–45]	t_{32}	transformation of monocytes into tissue macrophages	[3]
t_4	Ro60 protein expression	[42]	t_{33}	stimulation of foam cell formation	[3, 46]
t_5	DNA replication initiation and RNA quality control	[42]	t_{34}	stimulation of atherosclerotic plaque formation	[3, 46]
t_6	TLR7 receptor activation	[17, 42, 47]	t_{35}	progression of atherosclerotic lesions	[3, 17, 42, 45]
t_7	release of the sRNY Ro60 complex into the ECM (extracellular matrix)	[17]	t_{36}	IL-6R expression	[48]
t_8	internalization of the complex by the macrophage	[17]	t_{37}	MCP1 transcription	[3, 17, 22, 45]
t_9	TLR7 MyD88 binding	[3, 17, 22, 42]	t_{38}	reaction catalyzed by NAPDH oxidase	[43, 44]
t_{10}	TLR7 MyD88 IRAK4 binding	[3, 17, 22, 42]	t_{39}	increase in pro-inflammatory response	[3, 17, 22, 45, 46]
t_{11}	TLR7 MyD88 IRAK4 IRAK1 binding	[3, 17, 22, 42]	t_{40}	trapping of ox-LDL by macrophages	[3, 17, 45]
t_{12}	IRAK1 phosphorylation	[3, 17, 22, 42]	t_{41}	endothelial dysfunction due to inflammation	[3, 45]
t_{13}	TLR7 MyD88 IRAK4 IRAK1 1P TRAF6 binding	[3, 17, 22, 42]	t_{42}	JAK kinase recruitment	[48]
t_{14}	dissociation of IRAK1 and IRAK4	[3, 17, 22, 42]	t_{43}	Il6 gene transcription	[3, 17, 22, 45, 49]
t_{15}	activation of the IKK complex	[3, 17, 22, 42]	t_{44}	binding of JAK with the receptor for IL-6	[48]
t_{16}	I-κB phosphorylation (I-κB NF-κB complex)	[3, 17, 22, 42]	t_{45}	phosphorylation and activation of STAT3 and MAPK	[48]
t_{17}	I-κB dissociation from the I-κB NF-κB complex	[3, 17, 22, 42]	t_{46}	IL-6R IL-6 binding	[48]
t_{18}	ubiquitination and degradation of I-κB P	[3, 17, 22, 42]	t_{47}	processes leading to atherosclerotic plaque rupture	[3, 46]
t_{19}	NF-κB translocation to the nucleus	[3, 17, 22, 42]	t_{48}	expression of adhesion and pro-inflammatory molecules	[3, 17, 45, 49]
t_{20}	formation of the I-κB NF-κB complex and translocation into the cytoplasm	[3, 17, 22, 42]	t_{49}	MAPK kinase signaling pathway	[48]
t_{21}	I-κB gene transcription	[3, 17, 22, 42]	t_{50}	induction of MCP1 production	[3, 45]
t_{22}	I-κB and NF-κB expression	[3, 17, 22, 42]	t_{51}	expression of scavenger receptors	[3, 45]
t_{23}	TNF gene transcription	[3, 17, 22, 45, 49]	t_{52}	increased production of ROS (reactive oxygen species) and RNS (reactive nitrogen species) under the influence of various pathophysiological factors	[17, 43, 44]
t_{24}	apoptosis	[17, 42]	t_{53}	increased expression of scavenger receptors	[3, 17, 43–45]
t_{25}	caspase 3 activation	[42]	t_{54}	activation of NADPH oxidase	[3, 17, 43, 44, 46]
t_{26}	stimulation of caspase 3 activation	[42]	t_{55}	LDL formation	[3, 46]
t_{27}	iNOS gene transcription	[3, 17, 22]	t_{56}	iNOS activation induced by cytokines released from foam cells	[17]
t_{28}	nitric oxide synthesis	[17, 43, 44]			

(IL-6) (p_{34}, t_{43}), adhesion molecules (p_{25}, t_{30}; e.g., intercellular adhesion molecule-1 (ICAM-1), vascular cell adhesion molecule-1 (VCAM-1)), monocyte chemoattractant protein-1 (MCP-1) (p_{30}, t_{37}), and iNOS (inducible nitric oxide synthase) (p_{23}, t_{27}), thereby amplifying the inflammatory response (p_{21}, p_{34}, t_{23}, t_{39}). Additionally, NF-κB activates transcription of the I-κB gene (p_{19}, t_{21}), ensuring only transient activation of NF-κB (p_{18}, p_{19}, t_{20}, t_{21}) [3, 17, 22].

TLR7 stimulation (p_6, t_6) enhances macrophage uptake of ox-LDL (p_3, t_3, t_{40}) and reactive oxygen species (ROS) production (p_{22}, t_{38}, t_{53}, t_{54}), further promoting LDL oxidation. As a result of apoptosis (p_{43}, t_{24}) s-RNY/Ro60 complexes are released into the extracellular space (p_5, t_7), where they enter other macrophages (p_{27}, t_8), promoting inflammation (p_7–p_{19}, t_9–t_{22}, t_{39}) and apoptosis (p_{43}, t_{24}), thereby accelerating lesion progression (t_{35}) [17].

Experiments have shown that s-RNY (p_4) significantly enhances the expression of iNOS (p_{23}, p_{24}, t_{27}, t_{28}, t_{56}) and IL-6 (p_{34}, t_{43}, t_{48}) [17]. iNOS, unlike constitutive nNOS (neuronal nitric oxide synthase) and eNOS (endothelial nitric oxide synthase), is mainly induced by cytokines and lipopolysaccharides, producing nitric oxide (NO; p_{24}, t_{28}) continuously during inflammation. Although physiological NO generated by eNOS prevents LDL oxidation and leukocyte adhesion, pathological overproduction by iNOS leads to ROS (p_{22}, t_{38}, t_{53}, t_{54}), ox-LDL (p_3, t_3), excessive vasodilation and can contribute to cardiovascular failure (t_{29}) [43, 44].

IL-6 (p_{34}, t_{43}, t_{48}) is a multifunctional cytokine with predominantly pro-inflammatory effects, although it can also act anti-inflammatory depending on the cell context. Elevated IL-6 is observed in ischemic heart disease and myocardial infarction (t_{29}), in correlation with TNF-α (p_{21}, t_{23}) [45, 49]. Produced by endothelial cells (t_{41}), monocytes (p_{26}), and fibroblasts, IL-6 increases pro-inflammatory response (t_{39}), promotes MCP-1 production (p_{30}, t_{37}, t_{50}), enhances scavenger receptor expression (p_{40}, t_{51}, t_{53}), and accelerates ox-LDL uptake (p_3, t_3, t_{40}), contributing to atherosclerotic lesion progression (t_{35}) [3, 45]. By binding to IL-6R (p_{34}–p_{36}, t_{36}, t_{46}), IL-6 activates the Janus kinase/signal transducer and activator of transcription (JAK/STAT) (p_{32}, p_{33}, p_{38}, t_{42}, t_{44}, t_{45}) and mitogen-activated protein kinase (MAPK) (p_{39}, t_{45}, t_{49}) pathways, regulating adhesion molecule expression, proliferation, differentiation, and apoptosis [48].

2.3. Model construction and curation

The Petri net model was constructed in an evidence-driven and iterative manner, combining expert knowledge with a targeted literature search in accordance with the standard approach shown in Fig. 1. As a starting point, we used the study in [17]. It showed that small regulatory RNAs (s-RNY) derived from YRNA can serve as independent clinical biomarkers for detecting coronary artery lesions and are associated with atherosclerosis progression. The main dependencies reported there were as follows:

- The function of s-RNY is mediated by Toll-like receptor 7 (TLR7).

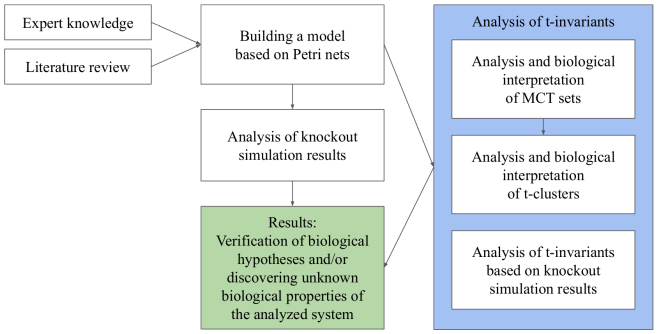

Fig. 1. A standard approach to modeling and analysis of complex biological systems using Petri nets

- The s-RNY/Ro60 complex activates TLR7, triggering NF-κB–dependent inflammation and caspase-3–dependent cell death.
- As a result of apoptosis, s-RNY/Ro60 complexes are released into the extracellular space, enter subsequent macrophages, and activate TLR7, thereby promoting apoptosis and inflammation in these cells.
- This feedback contributes to atherosclerosis progression.
- TLR7 stimulation increases macrophage uptake of oxLDL and enhances the production of reactive oxygen species (ROS), which in turn promotes further oxLDL formation.

Based on these relationships, we built an initial, minimal Petri net. Then we subsequently refined and extended it by systematically screening primary studies and review papers that expanded the above processes (described in detail, together with the supporting literature, in Section 2.2 and in the place/transition tables, i.e., Tables 1 and 2). For example, "ROS synthesis" was kept as a single transition because, in the present context, we considered detailed ROS generation mechanisms to be complex and unlikely to provide explanatory value proportional to the increase in model size. In contrast, we represented the activation of the nuclear factor κB (NF-κB) signalling pathway downstream of TLR7 in more detail. This includes recruitment of IRAK kinases, as it is part of the cascade that was explicitly mentioned in the main study [17]. Importantly, general nodes can always be expanded into more detailed subnetworks or linked to existing Petri net models via selected interface nodes.

Moreover, we did not directly reuse curated pathway resources (e.g., KEGG, Reactome) as model inputs. However, when the processes under consideration are represented in such resources (e.g., in KEGG), we routinely consult them as complementary references in our modelling workflow. It should be noted that transferring pathway maps (e.g., from KEGG) into a Petri net is not straightforward: Petri net models are typically specified at a much higher resolution, whereas pathway diagrams are often schematic and do not provide sufficient detail for a one-to-one mapping. In addition, pathway maps may not always reflect the most recent evidence. Moreover, regardless of their currency, translating such resources into a Petri net typically requires substantial manual curation (e.g., literature verification, gap filling, and consistent naming of entities and interactions).

Accordingly, interactions were included if supported by experimental evidence in the relevant biological context or if consistently described in authoritative reviews. Candidate edges were pruned when support was weak or when they were redundant, given the chosen abstraction level.

Finally, t-invariant–based checks were used to verify that the network reproduces the expected qualitative dependencies and to identify areas requiring further refinement. In particular, we required the net to be covered by t-invariants.

3. RESULTS

3.1. Presentation of the model and results of its formal analysis

This section presents a mathematical model based on Petri net theory. The network was developed using Holmes tool [50] and is shown in Fig. 2. It consists of 44 places and 57 transitions, which numbers with their assigned names are described in Tables 1 and 2, respectively.

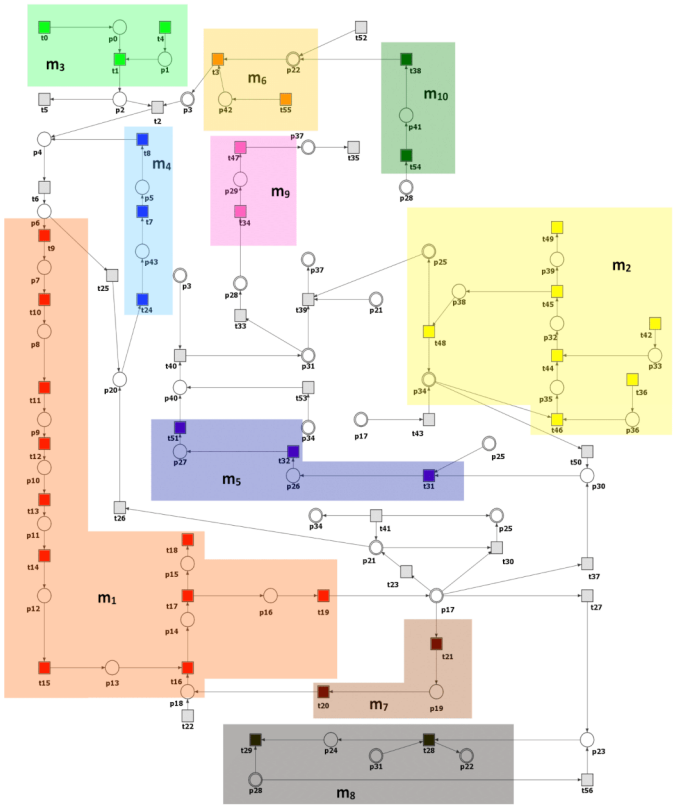

Fig. 2. Petri net model illustrating the role of YRNA-derived s-RNAs in the regulation of apoptosis and inflammatory process in monocytes/macrophages. Non-trivial MCT sets have been highlighted by framing and appropriate labeling. Transitions within each MCT set are shown as color-filled rectangles. Logical places, which are graphical representations of the same place in the network, are marked with double circles

Structural analysis of the model was carried out using the Holmes tool. In terms of structural properties, the network is pure, as it contains no reading arcs (connections where the substrate is not consumed), and ordinary, as the weights of all arcs are equal to 1. It is also connected, but not strongly connected, because there is no directed path between some pairs of vertices. The model is not structurally conflict-free, as it contains transitions with common input places (e.g., t_9 and t_{25}). It is also not conservative, as it has input transitions (without pre-places, e.g., t_0, t_4) and output transitions (without post-places, e.g., t_5, t_{35}). In addition, the presence of transitions without input and output places, which can insert any number of tokens into the network at their successor places, makes the network unbounded.

The analysis showed that the network is fully covered by 82 t-invariants and contains no minimal p-invariants. Therefore, further research was focused on the analysis of t-invariants.

The next step in the analysis was to generate MCT sets based on a set of t-invariants. They divide the network structure into separate areas that have specific biological functions within the modeled system. 10 non-trivial MCT sets (containing at least two transitions) were identified in the network, and their characteristics are presented in Table 3.

Table 3
Characteristics of the MCT sets of the network model

MCT sets	List of transitions	Biological meaning
m_1	t_9, t_{10}, t_{11}, t_{12}, t_{13}, t_{14}, t_{15}, t_{16}, t_{17}, t_{18}, t_{19}	MyD88-dependent TLR7 signal pathway
m_2	t_{36}, t_{42}, t_{44}, t_{45}, t_{46}, t_{48}, t_{49}	Activation of JAK/STAT, MAPK kinase signaling pathway and IL-6-mediated regulation of adhesion molecule expression
m_3	t_0, t_1, t_4	Binding of YRNA to Ro60 protein and formation of RoRNP complex
m_4	t_7, t_8, t_{24}	Release of sRNY-Ro60 complexes by apoptosis into the extracellular space and their internalization by macrophages
m_5	t_{31}, t_{32}, t_{51}	Recruitment of monocytes and their transformation into activated macrophages
m_6	t_3, t_{55}	The process of lipid peroxidation in LDL particles
m_7	t_{20}, t_{21}	The process of inhibition of NF-κB activity
m_8	t_{28}, t_{29}	Effects of nitric oxide on the cardiovascular system
m_9	t_{34}, t_{47}	Progression of changes within the atherosclerotic plaque
m_{10}	t_{38}, t_{54}	The process of ROS synthesis by NADPH oxidase

In the next stage of the analysis, the clustering was performed using the UPGMA algorithm, based on the average linkage method [51]. Pearson's correlation was used as a similarity measure and the number of clusters was chosen using the MSS index.

As a result, the set of t-invariants was divided into 7 t-clusters (see Fig. 3), the biological meaning of which is shown in Table 4.

Table 4
List of 7 clusters with biological description

Cluster	Biological meaning	Size	Transitions/ MCT sets
c_1	The formation of the RoRNP complex and the role of YRNA in the initiation of DNA replication and RNA quality control	1	m_3, t_5
c_2	Processes associated with the release of sRNY-Ro60 complexes into the extracellular space occurring as a result of apoptosis dependent on caspase 3 activity	1	m_4, t_6, t_{25}
c_3	Processes involved in the release of sRNY-Ro60 complexes into the extracellular space and activation of the MyD88-dependent TLR7 signaling pathway leading to TNF-dependent apoptosis	1	$m_1, m_4, t_6, t_{22}, t_{23}, t_{26}$
c_4	Processes leading to the progression of atherosclerotic lesions with special emphasis on the processes associated with lipid peroxidation in LDL particles	1	$m_6, t_{35}, t_{39}, t_{40}, t_{41}, t_{52}, t_{53}$
c_5	Processes leading to the progression of atherosclerotic lesions with special emphasis on the JAK/STAT signaling pathway	1	$m_2, m_5, m_6, t_{35}, t_{39}, t_{40}, t_{41}, t_{50}, t_{52}$
c_6	The core integrated disease process, encompassing the processes leading to the formation of the sRNY-Ro60 complex and its influence on the progression of atherosclerotic lesions occurring as a result of activation of the MyD88-dependent TLR7 signaling pathway	45	$m_1, m_2, m_3, m_5, m_6, m_7, m_8, m_9, m_{10}, t_2, t_6, t_{22}, t_{23}, t_{27}, t_{30}, t_{33}, t_{35}, t_{37}, t_{39}, t_{40}, t_{41}, t_{43}, t_{50}, t_{52}, t_{53}, t_{56}$
c_7	Processes leading to the release of the sRNY-Ro60 complex into the extracellular space and its effect on the progression of atherosclerotic lesions occurring as a result of activation of the MyD88-dependent TLR7 signaling pathway	32	$m_1, m_2, m_3, m_4, m_5, m_6, m_7, m_8, m_9, m_{10}, t_2, t_6, t_{22}, t_{26}, t_{27}, t_{30}, t_{33}, t_{35}, t_{37}, t_{39}, t_{40}, t_{41}, t_{43}, t_{50}, t_{52}, t_{53}, t_{56}$

The analysis confirmed that TLR7 receptor stimulation by sRNA-Ro60 complexes (extracellular and intracellular) and activation of two major signaling pathways – leading to inflammation and apoptosis – have a significant impact on the progression of atherosclerosis. These processes mainly belong to the two largest clusters (c_6 and c_7) and smaller clusters containing single t-invariants (c_1, c_2, c_3). Notably, the largest c_6 cluster represents the core integrated disease process. It encompasses processes

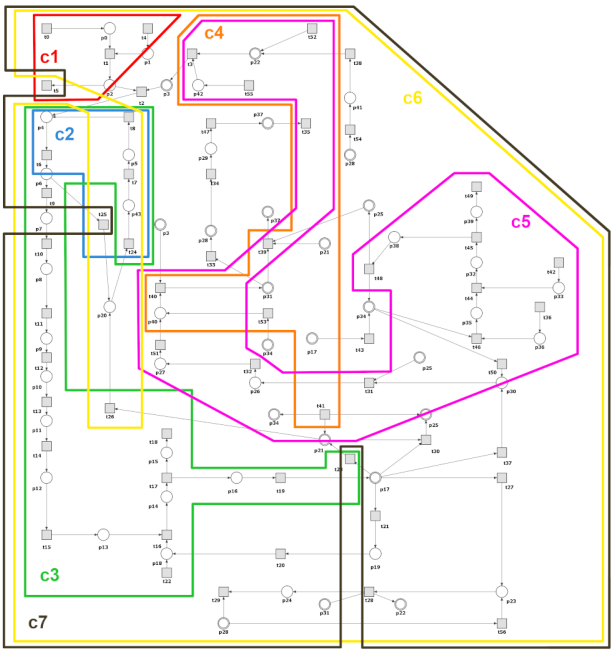

Fig. 3. Graphical depiction of t-clusters. Each t-cluster is highlighted with a frame and appropriate labeling

leading to the formation of the sRNY–Ro60 complex and its influence on the progression of atherosclerotic lesions occurring as a result of activation of the MyD88-dependent TLR7 signalling pathway. Other clusters include oxidative stress-dependent processes (c_4) and activation of the JAK/STAT pathway (c_5), associated with stimulation of the expression of adhesion and pro-inflammatory molecules.

The results of this analysis highlighted a complex network of relationships between apoptosis, inflammation, and activation of sRNA-Ro60 complexes, which are involved in almost all the key atherosclerotic processes described in Table 4.

The clustering results did not prove to be fully satisfactory. The analysis yielded two large clusters that encompass almost the entire network (94% of all t-invariants) and five clusters that contain only one t-invariant each (see Table 4). This outcome appears to be a unique feature of the system under consideration, suggesting that the modeled processes are strongly interdependent and interconnected.

3.2. The biological questions we answered using the knockout analyses

To achieve a complete and accurate biological interpretation of the network, further analyses were required. For this reason, two types of knockout analysis were performed: one based on the set of t-invariants and the other on simulation. The simulation was performed by disabling specific transitions and recording transition firings in 100 000 steps. This process was repeated 100 times, and the average number of transition firings and token accumulations was then calculated.

Scenario 1. Investigation of the importance of each functional biological unit (MCT set) and selected transitions in the studied model

The aim of this analysis was to determine the impact of disabling individual transitions in the network on the set of t-invariants and, indirectly, on other transitions within the modeled system. The analysis was carried out using the MonaLisa software [52].

This type of analysis was performed to assess the impact of sRNY–Ro60 complexes (both extracellular and intracellular), acting through TLR7 activation, on the progression of atherosclerotic lesions.

The formation of sRNY–Ro60 complexes occurs in response to atherogenic factors such as ox-LDL. As shown in Table 5, disabling transitions belonging to MCT set m_6 (the process of lipid peroxidation in LDL particles) has a major effect on the modeled system. These transitions are included in the supports of 79 out of 82 computed t-invariants. Their knockout halts lesion progression by blocking the production of ROS and sRNY–Ro60 complexes. It prevents TLR7 activation and the subsequent signaling pathway that amplifies the pro-inflammatory response.

Table 5

The impact of disabling individual transitions on the set of t-invariants and, indirectly, on other transitions within the modeled system. Single transitions (trivial MCT sets) are denoted as t, whereas non-trivial MCT sets are denoted as m. Transitions whose knockout did not affect other transitions in the analyzed network were omitted

MCT sets	Activity	Affected transitions	Affected t-invariants
t_{52}	Increased production of ROS and RNS under the influence of various pathophysiological factors	67.74%	87.80%
m_6	The process of lipid peroxidation in LDL particles	57.89%	96.34%
t_6	TLR7 receptor activation	57.89%	96.34%
m_1	MyD88-dependent TLR7 signal pathway	49.12%	95.12%
t_{40}	Trapping of ox-LDL by macrophages	47.37%	95.12%
t_{33}	Stimulation of foam cell formation	14.04%	84.15%
m_2	Activation of JAK/STAT, MAPK kinase signaling pathway and IL-6-mediated regulation of adhesion molecule expression	10.53%	24.39%
t_{22}	I-κB i NF-κB	8.77%	90.24%
m_5	Recruitment of monocytes and their transformation into activated macrophages	7.02%	86.59%
m_3	Binding of YRNA to Ro60 protein and formation of RoRNP complex	7.02%	56.10%
m_4	Release of sRNY-Ro60 complexes by apoptosis into the extracellular space and their internalization by macrophages	7.02%	42.68%
m_8	Effects of nitric oxide on the cardiovascular system	5.26%	42.68%
t_{35}	Progression of atherosclerotic lesions	5.26%	39.02%
m_7	The process of inhibition of NF-κB activity	1.75%	6.10%
m_9	Progression of changes within the atherosclerotic plaque	1.75%	20.73%
m_{10}	The process of ROS synthesis by NADPH oxidase	1.75%	20.73%

A similar effect is observed when the transition t_{52} (increased production of ROS and RNS (reactive nitrogen species) under the influence of various pathophysiological factors) is disabled. Blocking this transition prevents lipid peroxidation and consequently ox-LDL formation. Without ox-LDL, sRNY–Ro60 complexes cannot be generated and the processes driving atherosclerosis progression are interrupted. The results presented in Table 5 show that these blocked processes are represented by 72 of the 82 t-invariants.

Transition t_{35} (progression of atherosclerotic lesions) is included in the supports of 32 out of 82 t-invariants. Disabling transition t_6 (TLR7 receptor activation) results in 30 of them being eliminated, leaving only 2 active. Of these two remaining t-invariants, both are associated with lesion progression, one through oxidative stress and the other via activation of the JAK/STAT signaling pathway.

Scenario 2. Effect of Interleukin-6 (IL-6) on apoptosis and the progression of atherosclerotic lesions.

To investigate the impact of inhibiting IL-6 on apoptosis and the progression of atherosclerotic lesions, we disabled the following transitions: t_{41} (endothelial dysfunction due to inflammation), t_{43} (Il6 gene transcription), and t_{48} (expression of adhesion and pro-inflammatory molecules). As a result of the analysis, the number of t-invariants contributing to atherosclerosis progression decreased from 32 to 2, indicating a strong attenuation of this process. In the baseline net without any knockout, there are 82 t-invariants, 32 of which contribute to the progression of atherosclerosis (t_{35} (progression of atherosclerotic lesions)).

Next, the role of oxidative stress in atherosclerosis was also examined. To account for this, transition t_{52} (increased production of ROS and RNS under the influence of various pathophysiological factors) was also excluded from the model. As expected, combined anti-inflammatory and antioxidative treatment led to inhibition of atherosclerosis (see Fig. 4).

It is worth noting that inhibition of IL-6 simultaneously causes a decrease in apoptosis (see Fig. 4), with the number of t-invariants for the apoptosis transition t_{24} (apoptosis) decreasing from 35 to 2. This result is consistent with the literature on other studies, which have shown, among other things, that interleukin-6 plays a crucial role in the pathogenesis and progression of cancers. Specifically, it facilitates tumor growth by inhibiting cellular apoptosis and inducing angiogenesis within the tumor [53]. It has also been shown to protect cells from apoptosis during infection and inflammation [54].

Additionally, a stoppage in nitric oxide production (t_{27} (iNOS gene transcription)) was observed (see Fig. 2), which aligns with reports that IL-6 increases iNOS expression [55].

Scenario 3. The impact of the s-RNY/Ro60 complex on the progression of atherosclerosis

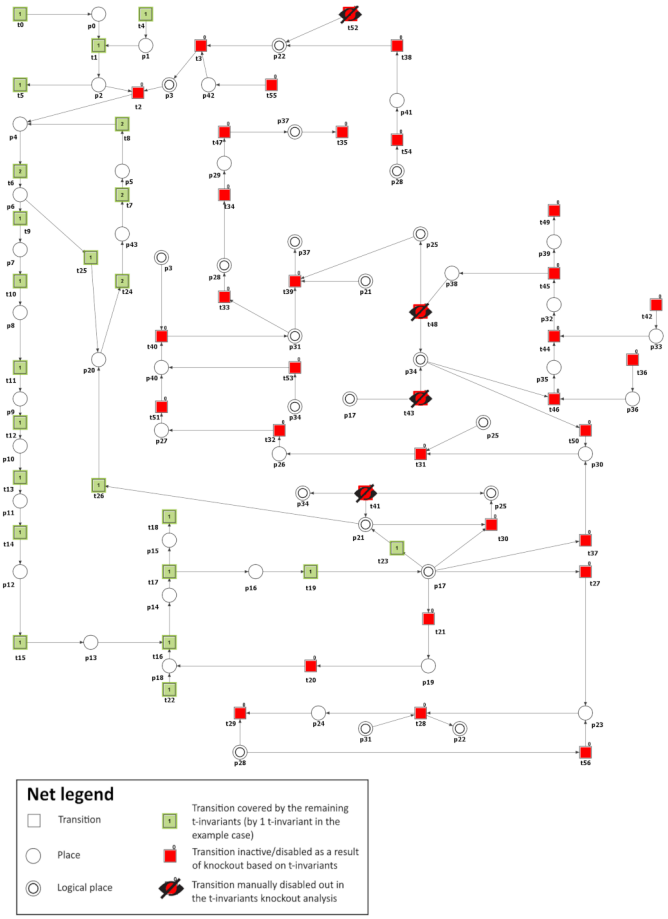

Fig. 4. Graphical depiction of the knockout effect of the following transitions: t_{41} (endothelial dysfunction due to inflammation), t_{43} (Il6 gene transcription), t_{48} (expression of adhesion and pro-inflammatory molecules) and t_{52} (increased production of ROS and RNS under the influence of various pathophysiological factors). Transitions inactivated in the knockout simulation are shown as crossed-out black circles. Transitions in the t-invariant's support are marked with solid green rectangles [50]

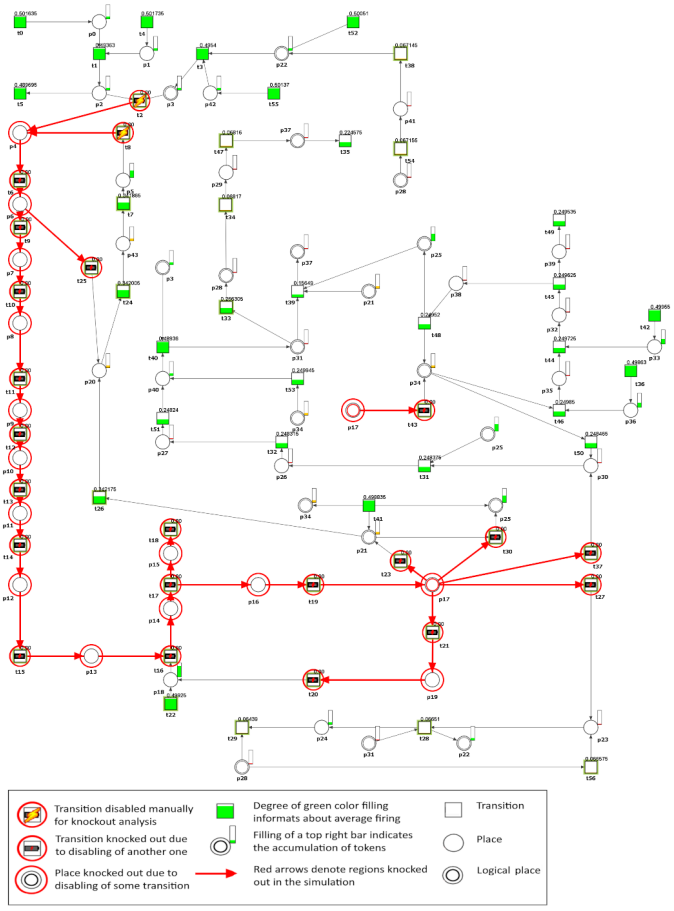

Fig. 5. Graphical representation of the knockout effect on apoptosis and atherosclerosis progression, focusing on transitions t_2 (degradation of YRNA to sRNA) and t_8 (internalization of the complex by the macrophage). Inactive transitions are shown as red circles, while active ones are depicted as green or yellow rectangles, depending on activity change

To more precisely assess the impact of the s-RNY/Ro60 complex on the progression of atherosclerotic lesions, the following transitions were disabled: t_2 (degradation of YRNA to sRNA) and t_8 (internalization of the complex by the macrophage) (see Fig. 5). Consequently, it can be observed in Fig. 5 that the transition t_{27} (transcription of the iNOS gene), representing NF-κB–dependent iNOS gene expression, is indirectly inactivated. However, transition t_{56} (iNOS activation induced by cytokines released from foam cells) and t_{28} (nitric oxide synthesis) remain active, influenced by ox-LDL–loaded macrophages (p_{31}) and the presence of reactive oxygen and nitrogen species (p_{22}).

Since the processes associated with atherogenesis and the pro-inflammatory response are not fully halted and continue to occur, particularly under oxidative stress, macrophages remain stimulated, leading to sustained iNOS expression and, consequently, nitric oxide production.

Furthermore, if transition t_{52} (increased ROS/RNS production under pathophysiological conditions), representing reactive oxygen species generated by various pathophysiological processes, is deactivated, the progression of atherosclerosis represented by t_{35} (progression of atherosclerotic lesions) is stopped (see Fig. 6).

It is worth noting that the same effect can be achieved by the knockout of the following transitions: t_6 (TLR7 receptor activation) and t_{52} (increased ROS/RNS production under pathophysiological conditions).

3.3. Limitations of the study

Effective Petri-net modeling of complex biological systems requires certain level of abstraction, given the inherent complexity and the many underlying processes. Since not all pathways can be represented, some simplifications are needed to keep the model manageable and computationally feasible.

Classical network models mainly describe system structure, which is essential for understanding their functionality. This qualitative approach helps identify key components and interactions despite simplifying real complex processes. It may not capture all interactions or the full range of dynamics, especially

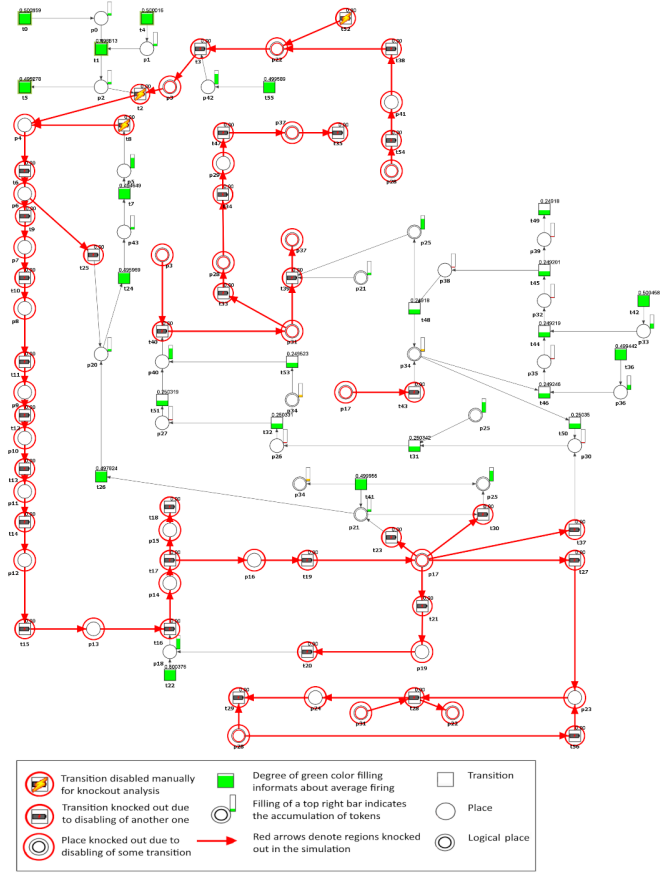

Fig. 6. Graphical representation of the knockout effect on apoptosis and atherosclerosis progression, focusing on transitions t_2 (degradation of YRNA to sRNA), t_8 (internalization of the complex by the macrophage) and t_{52} (increased ROS/RNS production under pathophysiological conditions). Inactive transitions are shown as red circles, while active ones are depicted as green or yellow rectangles, depending on activity change

time-dependent changes. Such models do not represent stochasticity, discrete biomolecule counts, or concentration-dependent kinetics. Therefore, they cannot capture threshold effects, dose-response relationships or variability between cells and individuals. Relatedly, feedback loops are encoded only at the level of network topology. Thus, without explicit time or quantitative state variables, the model cannot reproduce dynamical features such as delays, oscillations, transient activation, or time-dependent accumulation/depletion of intermediates. Moreover, simulated in silico knockouts may not accurately reproduce the effects of real interventions in these systems.

Another important limitation concerns biological detail and scale. The model integrates low-level molecular events (e.g., phosphorylation steps) with higher-level, phenomenological transitions (e.g., progression of atherosclerotic lesions). It necessitates certain simplifications and may limit broader interpretation. Furthermore, spatial aspects of atherosclerosis, such as vessel wall anatomy, compartmentalisation, diffusion, gradients, and localisation, are not explicitly modelled. Cellular heterogeneity (distinct macrophage, endothelial, and smooth muscle cell states, recruitment and differentiation, microenvironmental variation) is also represented only implicitly, which limits conclusions about cell-type-specific contributions and multicellular organisation.

Importantly, there exist many extensions of classical Petri nets that enable incorporating quantitative information, such as timing constraints or kinetic rates, thereby increasing model precision and allowing a more detailed investigation of system properties. Among them are Time Petri nets, which support modelling of process duration by assigning a delay to each transition, and Stochastic Petri nets, which account for reaction probabilities by associating a firing rate with each transition, describing both the likelihood and frequency of transition firings. Such quantitative extensions are natural and typically require only adding quantitative annotations without modifying the underlying network structure. For these Petri net variants, the analysis steps described for the classical model remain applicable. It should be noted, however, that exact time dependencies between components of the modelled processes and kinetic constants are often unknown and difficult to reliably infer from the available literature.

Despite these limitations, network models are useful for revealing system properties and guiding experimental work. Accordingly, the model predictions should be treated as qualitative hypotheses and prioritised for experimental validation (e.g., in cell culture or animal models). Nevertheless, comprehensive experimental validation in all aspects of complex long-term diseases such as atherosclerosis may not always be practical or feasible.

4. DISCUSSION

With advances in sequencing technologies, an increasing number of functionally important noncoding RNAs have been identified across many diseases [31, 56]. For example, in cardiovascular disease (CVD), vascular smooth muscle cell (VSMC) phenotypic switching is accompanied by tissue-specific expression of multiple miRNAs [56]. These miRNAs also regulate VSMC migration stimulated by the RhoA/ROCK axis, which plays a crucial role in diverse cellular processes, including cytoskeletal organization, cell migration, proliferation, and apoptosis [56].

In parallel, YRNA–derived small RNAs (s-RNYs), identified by small-RNA high-throughput sequencing have emerged as independent clinical biomarkers of coronary artery lesions and are associated with atherosclerotic burden [5, 6, 17]. Despite this progress, links between the molecular mechanisms of atherosclerosis and small RNAs remain limited. However, this line of research is crucial, as their analysis opens new opportunities to define regulatory events in pathophysiology [30, 31].

To translate the knowledge and the results of numerous experiments reported in the literature into system-level mechanisms, the first, and essential step in studying a complex system is to build a formal, mathematically defined model. Although differential equations have been the traditional choice, graph- and network-based approaches are increasingly used because they naturally capture relationships among system components. Petri nets are particularly promising because their structure

aligns well with biological systems and their graphical notation supports intuitive model construction and interpretation. Additionally, there is a mature toolkit of mathematical methods and software for analyzing their properties, which correspond to biological features of the system [50, 51, 57].

Despite extensive insight into the inflammatory, oxidative, and lipid dysregulation that underlie atherosclerosis, effective therapy remains challenging. We therefore adopted a system approach to better understand this problem and elucidate how YRNA-derived small RNAs (s-RNYs) intersect lipid peroxidation, innate immune signaling, and oxidative stress to drive atherogenesis.

However, modeling such a complex network of interacting processes required certain simplifications, and not all mechanisms could be included. For example, we did not model cholesterol and lipoprotein metabolism in its full complexity, limiting this part of the network to ox-LDL formation via lipid peroxidation, as ox-LDL is a crucial atherogenic stimulus. Importantly, the network can be expanded by replacing selected nodes with dedicated subnetworks that represent the corresponding processes in greater mechanistic detail. For instance, the current network could be coupled with our previously proposed model [40], which would allow incorporation of recent findings on the heterogeneous composition and functional diversity of HDL particles, including evidence that increasing HDL beyond a certain threshold may reverse its protective role and potentially exacerbate CVD [58].

To our knowledge, no prior study has examined small noncoding RNAs in atherosclerosis by simultaneously integrating, within a single project, the many signaling pathways and fundamental processes that shape this complex disease. We viewed atherosclerosis as a network of interconnected interactions in which blocking one pathway can impact others. Thanks to this, we have been able to identify the most crucial pathways that must be blocked to stop the progression of this disease.

To this end, we analyzed a Petri-net–based model using t-invariant analysis, in silico knockouts of selected subnetworks, and dynamic simulations. Because s-RNY–Ro60 complexes form in response to atherogenic stimuli such as ox-LDL [18], we tested whether blocking s-RNYs (e.g., with complementary oligonucleotides) would prevent activation of the NF-$\kappa\beta$–dependent pathway and, in turn, slow the development of atherosclerotic lesions. The progression was attenuated but not eliminated. Given the multifactorial nature of atherosclerosis, oxidative stress also had to be inhibited, indicating that simultaneous suppression of this process is required to halt disease progression. This is consistent with the literature, as the NF-$\kappa\beta$ pathway and oxidative stress are tightly interconnected [59]. Thus, a potential therapeutic strategy here could combine antioxidant approaches with antisense oligonucleotides targeting Ro-associated non-coding RNAs [60].

Similarly, the model predicts that combining TLR7-receptor blockade with neutralization of ROS/RNS sources consistently halts atherosclerosis progression. This requirement for dual targeting is one of the insights of this work, as single-target interventions are insufficient, even when NF-$\kappa\beta$–dependent pathway is silenced.

Oxidative stress is a well-known component of atherosclerosis pathogenesis, occurring in parallel with activation of proinflammatory signaling. Among key mediators, IL-6 is a proinflammatory, pro-atherogenic cytokine that promotes plaque progression and destabilization. In humans, endothelial cells produce IL-6, which colocalizes with angiotensin II in aortic atherosclerotic plaques [61]. Consistent with this, murine studies have shown that IL-6 increases peripheral platelet counts (thrombocytosis), modulates endothelium-dependent relaxation, influences vascular monocyte differentiation, and affects metabolism related to obesity. IL-6 also induces the expression of tissue factor in monocytes with increased procoagulant activity, an effect reversible after IL-6 withdrawal. Targeted IL-6 inhibition has also been shown to deserve careful consideration. Patients with end-stage renal disease have a markedly elevated atherothrombotic risk and a heightened inflammatory response, further amplified by hemodialysis [61, 62], while statin efficacy is limited. Together, these factors underscore the urgent need for new atheroprotective therapies and warrant investigation of the IL-6 pathway inhibition.

For this reason, we investigated whether inhibiting IL-6 could slow the progression of atherosclerotic lesions. We found that disease progression was attenuated but not stopped. As in the other scenarios, concurrent suppression of oxidative stress was also required.

Since oxidative stress had to be suppressed across all tested intervention scenarios, it represents a broadly necessary component for halting lesion progression in our model. Therefore, we next considered other pharmacological candidates with the potential to attenuate oxidative stress–associated inflammatory signaling cascades. In this context, increasing attention has been directed toward plant-derived or plant-inspired small molecules, including flavonoids, as potential modulators of atherosclerosis. Among these compounds, 7-O-methyldihydropunctatin (MP), a plant-derived homoisoflavonoid, has recently been proposed as a candidate anti-atherosclerotic agent [63, 64]. Recent computational studies have suggested arachidonate 5-lipoxygenase (ALOX5) as a likely molecular target of MP [64]. ALOX5 is involved in the biosynthesis of inflammatory lipid mediators such as leukotrienes, which play a central role in recruiting and activating immune cells (e.g., neutrophils and macrophages) at sites of inflammation, and it is also linked to pathways that amplify oxidative stress through increased ROS generation [65–68]. In accordance with these mechanistic considerations, MP and other ALOX5-targeting inhibitors have been reported to attenuate atherosclerosis progression, supporting MP as a promising therapeutic candidate [64, 67, 69].

Overall, using in silico knockouts of selected pathways, we examined how different combinations of commonly used drugs influence atherosclerosis. Petri net–based models, by enabling detailed representations of biological systems, even when comprising dozens or hundreds of elementary components, make such virtual interventions possible and support systematic testing of therapeutic options [39, 40]. Consistent with these analyses, we find that most pathogenic processes in our model can be attenuated with dual-target knockouts: suppression of reactive oxygen and nitrogen species (ROS/RNS) generated by diverse

pathophysiological processes paired with inhibition of either (1) the TLR7 receptor, (2) s-RNYs, or (3) the pro-inflammatory cytokine IL-6. Together, these results position multi-pathway combination therapy as a promising route to more effective treatment of atherosclerosis.

5. CONCLUSIONS

The obtained results confirm that blocking the TLR7 receptor (e.g., using chloroquine) or s-RNY (e.g., through complementary oligonucleotides) prevents activation of the NF-κB–dependent signaling pathway. At the same time, although NF-κB signaling is inactivated, lesion progression is not reduced. This is because atherosclerosis is a complex, multifactorial disease in which additional factors, such as ROS and RNS, also influence its course and development.

Only when ROS (reactive oxygen species) and RNS (reactive nitrogen species), generated by various pathophysiological processes, are simultaneously eliminated, can inhibition of atherosclerotic lesion progression be observed.

Direct blockade of the inflammatory response by inhibiting the pro-inflammatory cytokine IL-6 markedly reduces the progression of atherosclerotic lesions but, similar to s-RNA or TLR7 inhibition, does not fully halt it. When oxidative stress is additionally reduced, further progression of atherosclerosis is stopped. At the same time, apoptosis decreases but does not completely cease, consistent with the literature [53, 54].

Taken together, our analysis indicates that combination therapy, using agents that target key components of the modeled network (1) the TLR7 receptor, (2) s-RNY, or (3) the pro-inflammatory cytokine IL-6, together with blockade of oxidative stress, made it possible to control the development and progression of atherosclerosis in the proposed model.

REFERENCES

[1] V. Tasouli-Drakou, I. Ogurek, T. Shaikh, M. Ringor, M. DiCaro, and K. Lei, "Atherosclerosis: A comprehensive review of molecular factors and mechanisms," *Int. J. Mol. Sci.*, vol. 26, no. 3, p. 1364, 2025, doi: 10.3390/ijms26031364.

[2] I. Razeghian-Jahromi, A. Karimi Akhormeh, M. Razmkhah, and M. Zibaeenezhad, "Immune system and atherosclerosis: Hostile or friendly relationship," *Int. J. Immunopathol. Pharmacol.*, vol. 36, 2022, doi: 10.1177/03946320221092188.

[3] A. Tedgui and Z. Mallat, "Cytokines in atherosclerosis: Pathogenic and regulatory pathways," *Physiol. Rev.*, vol. 86, no. 2, pp. 515–581, 2006, doi: 10.1152/physrev.00024.2005.

[4] K. Guglas *et al.*, "YRNAs and YRNA-derived fragments as new players in cancer research and their potential role in diagnostics," *Int. J. Mol. Sci.*, vol. 21, no. 16, p. 5682, 2020, doi: 10.3390/ijms21165682.

[5] W. Chen *et al.*, "Extracellular vesicle YRNA in atherosclerosis," *Clin. Chim. Acta*, vol. 517, pp. 15–22, 2021, doi: 10.1016/j.cca.2021.02.003.

[6] N. Valkov and S. Das, "Y RNAs: Biogenesis, function and implications for the cardiovascular system," *Adv. Exp. Med. Biol.*, vol. 1229, pp. 327–342, 2020, doi: 10.1007/978-981-15-1671-9_20.

[7] M.N. Hasan, M.M. Rahman, A.A. Husna, N. Nozaki, O. Yamato, and N. Miura, "YRNA and tRNA fragments can differentiate benign from malignant canine mammary gland tumors," *Biochem. Biophys. Res. Commun.*, vol. 691, p. 149336, 2024, doi: 10.1016/j.bbrc.2023.149336.

[8] T.A.P. Driedonks and E.N.M. Nolte-'t Hoen, "Circulating Y-RNAs in extracellular vesicles and ribonucleoprotein complexes; implications for the immune system," *Front. Immunol.*, vol. 9, p. 3164, 2019, doi: 10.3389/fimmu.2018.03164.

[9] W. Yang, X. Pan, and A. Ma, "The potential of exosomal rnas in atherosclerosis diagnosis and therapy," *Front. Neurol.*, vol. 11, p. 572226, 2021, doi: 10.3389/fneur.2020.572226.

[10] Z. Wehbe *et al.*, "Emerging understandings of the role of exosomes in atherosclerosis," *J. Cell. Physiol.*, vol. 240, no. 1, p. e31454, 2025, doi: 10.1002/jcp.31454.

[11] Y. Zhang, J. Bi, J. Huang, Y. Tang, S. Du, and P. Li, "Exosome: a review of its classification, isolation techniques, storage, diagnostic and targeted therapy applications," *Int. J. Nanomed.*, vol. 15, pp. 6917–6934, 2020, doi: 10.2147/IJN.S264498.

[12] J. Heo and H. Kang, "Exosome-based treatment for atherosclerosis," *Int. J. Mol. Sci.*, vol. 23, no. 2, p. 1002, 2022, doi: 10.3390/ijms23021002.

[13] M. Sopic *et al.*, "Transcriptomic research in atherosclerosis: Unravelling plaque phenotype and overcoming methodological challenges," *J. Mol. Cell. Cardiol. Plus*, vol. 6, p. 100048, 2023, doi: 10.1016/j.jmccpl.2023.100048.

[14] L.W. McQueen *et al.*, "Next-generation and single-cell sequencing approaches to study atherosclerosis and vascular inflammation pathophysiology: a systematic review," *Front. Cardiovasc. Med.*, vol. 9, p. 849675, 2022, doi: 10.3389/fcvm.2022.849675.

[15] A. Hildebrandt *et al.*, "Detection of atherosclerosis by small RNA-sequencing analysis of extracellular vesicle-enriched serum samples," *Front. Cell Dev. Biol.*, vol. 9, p. 729061, 2021, doi: 10.3389/fcell.2021.729061.

[16] G. Nechooshtan, D. Yunusov, K. Chang, and T.R. Gingeras, "Processing by RNase 1 forms tRNA halves and distinct Y RNA fragments in the extracellular environment," *Nucleic Acids Res.*, vol. 48, no. 14, pp. 8035–8049, 2020, doi: 10.1093/nar/gkaa526.

[17] Z. Hizir, S. Bottini, V. Grandjean, M. Trabucchi, and E. Repetto, "Rny (yrna)-derived small rnas regulate cell death and inflammation in monocytes/macrophages," *Cell Death Dis.*, vol. 8, no. 1, p. e2530, 2017, doi: 10.1038/cddis.2016.429.

[18] H. Bai *et al.*, "The significance of small noncoding RNAs in the pathogenesis of cardiovascular diseases," *Genes Dis.*, vol. 12, no. 4, p. 101342, 2024, doi: 10.1016/j.gendis.2024.101342.

[19] M. Velázquez-Flores and R. Ruiz Esparza-Garrido, "Fragments derived from non-coding RNAs: how complex is genome regulation?" *Genome*, vol. 67, no. 9, pp. 292–306, 2024, doi: 10.1139/gen-2023-0136.

[20] J.M. Dhahbi, S.R. Spindler, H. Atamna, D. Boffelli, and D.I.K. Martin, "Deep sequencing of serum small RNAs identifies patterns of 5' tRNA half and YRNA fragment expression associated with breast cancer," *Biomark. Cancer*, vol. 6, pp. 37–47, 2014, doi: 10.4137/BIC.S20764.

[21] B.V. Martinez *et al.*, "Circulating small non-coding RNA signature in head and neck squamous cell carcinoma," *Oncotarget*, vol. 6, no. 22, pp. 19 246–19 263, 2015, doi: 10.18632/oncotarget.4266.

[22] T. Kawasaki and T. Kawai, "Toll-like receptor signaling pathways," *Front. Immunol.*, vol. 5, p. 461, 2014, doi: 10.3389/fimmu.2014.00461.

[23] W. Bargiel *et al.*, "Recognized and potentially new biomarkers – their role in diagnosis and prognosis of cardiovascular disease," *Medicina (Kaunas)*, vol. 57, no. 7, p. 701, 2021, doi: 10.3390/medicina57070701.

[24] A. Rybarczyk, D. Formanowicz, and P. Formanowicz, "The role of macrophage dynamics in atherosclerosis analyzed using a petri net-based model," *Appl. Sci.*, vol. 14, no. 8, p. 3219, 2024, doi: 10.3390/app14083219.

[25] A. Rybarczyk, D. Formanowicz, and P. Formanowicz, "Key therapeutic targets to treat hyperglycemia-induced atherosclerosis analyzed using a Petri Net-based model," *Metabolites*, vol. 13, no. 12, p. 1191, 2023, doi: 10.3390/metabo13121191.

[26] S. Pozzi, A. Redaelli, C. Vergara, E. Votta, and P. Zunino, "Mathematical modeling and numerical simulation of atherosclerotic plaque progression based on fluid–structure interaction," *J. Math. Fluid Mech.*, vol. 23, p. 74, 2021, doi: 10.1007/s00021-021-00598-8.

[27] S. Minucci, R. Heise, and A. Reynolds, "Agent-based vs. equation-based multi-scale modeling for macrophage polarization," *PLoS One*, vol. 19, p. e0270779, 2024, doi: 10.1371/journal.pone.0270779.

[28] A. Cohen, M. Myerscough, and R. Thompson, "Athero-protective effects of high-density lipoproteins (HDL): an ODE model of the early stages of atherosclerosis," *Bull. Math. Biol.*, vol. 76, pp. 1117–1142, 2014, doi: 10.1007/s11538-014-9948-4.

[29] S. Frei and A. Heinlein, "Towards parallel time-stepping for the numerical simulation of atherosclerotic plaque growth," *J. Comput. Phys.*, vol. 491, p. 112347, 2023, doi: 10.1016/j.jcp.2023.112347.

[30] X. He *et al.*, "Expression profiles and potential roles of transfer RNA-derived small RNAs in atherosclerosis," *J. Cell. Mol. Med.*, vol. 25, no. 14, pp. 7052–7065, 2021, doi: 10.1111/jcmm.16719.

[31] S. Greco, C. Gaetano, D. Mazzaccaro, and F. Martelli, "Circular RNA role in atherosclerosis development and progression," *Curr. Atheroscler. Rep.*, vol. 27, p. 60, 2025, doi: 10.1007/s11883-025-01306-x.

[32] T. Murata, "Petri nets: Properties, analysis and applications," *Proc. IEEE*, vol. 77, no. 4, pp. 541–580, 1989, doi: 10.1109/5.24143.

[33] D. Formanowicz, A. Kozak, and P. Formanowicz, "A Petri net based model of oxidative stress in atherosclerosis," *Found. Comput. Decis. Sci.*, vol. 37, no. 2, pp. 59–78, doi: 10.2478/v10209-011-0005-x.

[34] A. Sackmann, M. Heiner, and I. Koch, "Application of petri net based analysis techniques to signal transduction pathways," *BMC Bioinform.*, vol. 7, p. 482, 2006, doi: 10.1186/1471-2105-7-482.

[35] E. Grafahrend-Belau *et al.*, "Modularization of biochemical networks based on classification of petri net t-invariants," *BMC Bioinform.*, vol. 9, p. 90, 2008, doi: 10.1186/1471-2105-9-90.

[36] T. Caliński and J. Harabasz, "A dendrite method for cluster analysis," *Commun. Stat.*, vol. 3, pp. 1–27, 1974.

[37] P.J. Rousseeuw, "Silhouettes: A graphical aid to the interpretation and validation of cluster analysis," *J. Comput. Appl. Math.*, vol. 20, pp. 53–65, 1987.

[38] D. Formanowicz, M. Radom, A. Rybarczyk, and P. Formanowicz, "The role of fenton reaction in ros-induced toxicity underlying atherosclerosis – modeled and analyzed using a petri net-based approach," *Biosystems*, vol. 165, pp. 71–87, 2018, doi: 10.1016/j.biosystems.2018.01.002.

[39] D. Formanowicz, A. Rybarczyk, M. Radom, and P. Formanowicz, "A role of inflammation and immunity in essential hypertension – modeled and analyzed using Petri nets," *Int. J. Mol. Sci.*, vol. 21, no. 9, p. 3348, 2020, doi: 10.3390/ijms21093348.

[40] D. Formanowicz, M. Radom, A. Rybarczyk, K. Tanaś, and P. Formanowicz, "Control of cholesterol metabolism using a systems approach," *Biology*, vol. 11, no. 3, p. 430, 2022, doi: 10.3390/biology11030430.

[41] M. Radom, M.A. Machnicka, J. Krwawicz, J.M. Bujnicki, and P. Formanowicz, "Petri net–based model of the human dna base excision repair pathway," *PLoS One*, vol. 14, p. e0217913, 2019, doi: 10.1371/journal.pone.0217913.

[42] M. Mustafa *et al.*, "Apoptosis: A comprehensive overview of signaling pathways, morphological changes, and physiological significance and therapeutic implications," *Cells*, vol. 13, no. 22, p. 1838, 2024, doi: 10.3390/cells13221838.

[43] U. Förstermann, N. Xia, and H. Li, "Roles of vascular oxidative stress and nitric oxide in the pathogenesis of atherosclerosis," *Circ. Res.*, vol. 120, no. 4, pp. 713–735, 2017, doi: 10.1161/CIRCRESAHA.116.309326.

[44] P. Ryszkiewicz, E. Schlicker, and B. Malinowska, "Is inducible nitric oxide synthase (inos) promising as a new target against pulmonary hypertension?" *Antioxidants (Basel)*, vol. 14, no. 4, p. 377, 2025, doi: 10.3390/antiox14040377.

[45] A. Reiss, N. Siegart, and J. De Leon, "Interleukin-6 in atherosclerosis: atherogenic or atheroprotective?." *Clin. Lipidol.*, vol. 12, no. 1, pp. 14–23, 2017, doi: 10.1080/17584299.2017.1319787.

[46] E. Gusev and A. Sarapultsev, "Atherosclerosis and inflammation: Insights from the theory of general pathological processes," *Int. J. Mol. Sci.*, vol. 24, no. 9, p. 7910, 2023, doi: 10.3390/ijms24097910.

[47] R. Esparza-Garrido and M. Velázquez-Flores, "Activation of toll-like receptors by non-coding RNAs and their fragments (review)," *Mol. Med. Rep.*, vol. 32, no. 4, p. 285, 2025, doi: 10.3892/mmr.2025.13650.

[48] T. Takeda *et al.*, "Crosstalk between the interleukin-6 (IL-6)-JAK-STAT and the glucocorticoid-nuclear receptor pathway: synergistic activation of IL-6 response element by IL-6 and glucocorticoid." *J. Endocrinol.*, vol. 159, no. 2, pp. 323–330, 1998, doi: 10.1677/joe.0.1590323.

[49] J. Fuster and K. Walsh, "The Good, the Bad, and the Ugly of interleukin-6 signaling," *EMBO J.*, vol. 33, no. 13, pp. 1425–1427, 2014, doi: 10.15252/embj.201488856.

[50] M. Radom *et al.*, "Holmes: a graphical tool for development, simulation and analysis of petri net based models of complex biological systems," *Bioinformatics*, vol. 33, no. 23, p. 3822–3823, 2017, doi: 10.1093/bioinformatics/btx492.

[51] I. Koch, W. Reisig, and F. Schreiber, Eds., *Modeling in Systems Biology. The Petri Net Approach*. Springer London, 2011, doi: 10.1007/978-1-84996-474-6.

[52] J. Einloft, J. Ackermann, J. Nöthen, and I. Koch, "Monalisa – visualization and analysis of functional modules in biochemical networks," *Bioinformatics*, vol. 29, no. 11, pp. 1469–1470, 2013, doi: 10.1093/bioinformatics/btt165.

[53] Y. Liu, P. Li, C. Li, and J. Lin, "Inhibition of STAT3 signaling blocks the anti-apoptotic activity of IL-6 in human liver cancer cells," *J. Biol. Chem.*, vol. 285, no. 35, pp. 27 429–27 439, 2010, doi: 10.1074/jbc.M110.142752.

[54] J. Jin, X. Han, and Q. Yu, "Interleukin-6 induces the generation of IL-10-producing Tr1 cells and suppresses autoimmune tissue inflammation," *J. Autoimmun.*, vol. 40, pp. 28–44, 2013, doi: 10.1016/j.jaut.2012.07.009.

[55] J. Fontes, N. Rose, and D. Cihakova, "The varying faces of Il-6: from cardiac protection to cardiac failure," *Cytokine*, vol. 74, no. 1, pp. 62–68, 2015, doi: 10.1016/j.cyto.2014.12.024.

[56] T. Sawma *et al.*, "Role of rhoa and rho-associated kinase in phenotypic switching of vascular smooth muscle cells: Implications for vascular function," *Atherosclerosis*, vol. 358, pp. 12–28, 2022, doi: 10.1016/j.atherosclerosis.2022.08.012.

[57] E. Klipp, W. Liebermeister, C. Wierling, A. Kowald, H. Lehrach, and R. Herwig, *Systems Biology. A Textbook*. Weinheim: Wiley-VCH, 2009.

[58] M. Al Zein, A. Khazzeka, A. El Khoury, J. Al Zein, D. Zoghaib, and A.H. Eid, "Revisiting high-density lipoprotein cholesterol in cardiovascular disease: Is too much of a good thing always a good thing?" *Prog. Cardiovasc. Dis.*, vol. 87, pp. 50–59, 2024, doi: 10.1016/j.pcad.2024.10.009.

[59] A. Matsumori, "Nuclear factor-κB is a prime candidate for the diagnosis and control of inflammatory cardiovascular disease," *Eur. Cardiol. Rev.*, vol. 18, p. e40, Jun. 2023, doi: 10.15420/ecr.2023.10.

[60] A.V. Poznyak, A.V. Grechko, V.A. Orekhova, Y.S. Chegodaev, W.K. Wu, and A.N. Orekhov, "Oxidative stress and antioxidants in atherosclerosis development and treatment," *Biology*, vol. 9, no. 3, p. 60, 2020, doi: 10.3390/biology9030060.

[61] P.M. Ridker and M. Rane, "Interleukin-6 signaling and anti-interleukin-6 therapeutics in cardiovascular disease," *Circ. Res.*, vol. 128, no. 11, pp. 1728–1746, 2021, doi: 10.1161/CIRCRESAHA.121.319077.

[62] R. Pecoits-Filho, M.J. Carvalho, P. Stenvinkel, B. Lindholm, and O. Heimbürger, "Systemic and intraperitoneal interleukin-6 system during the first year of peritoneal dialysis," *Perit. Dial. Int.*, vol. 26, pp. 53–63, 2006, doi: 10.1177/089686080602600109.

[63] M. Fardoun *et al.*, "7-o-methylpunctatin, a novel homoisoflavonoid, inhibits phenotypic switch of human arteriolar smooth muscle cells," *Biomolecules*, vol. 9, no. 11, p. 716, 2019, doi: 10.3390/biom9110716.

[64] G. Elamin and A.H. Eid, "7-o-methylpunctatin is a potential inhibitor of human arachidonate 5-lipoxygenase: molecular and structural insights into anti-atherosclerosis therapeutics," *Mol. Divers.*, 2026, doi: 10.1007/s11030-025-11420-2.

[65] S. Kotlyarov, "Genetic and epigenetic regulation of lipoxygenase pathways and reverse cholesterol transport in atherogenesis," *Genes*, vol. 13, no. 8, p. 1474, 2022, doi: 10.3390/genes13081474.

[66] L. Wang and B. Wang, "ALOX5 regulates vascular smooth muscle cells pyroptosis to affect abdominal aortic aneurysm formation," *Sci. Rep.*, vol. 15, no. 1, p. 29123, doi: 10.1038/s41598-025-14268-6.

[67] Y. Chan *et al.*, "Effect of 5-lipoxygenase-activating protein inhibition on coronary atherosclerosis progression in patients with recent acute coronary syndrome: the passivate randomised clinical trial," *Eur. Heart J.*, vol. 46, no. Supplement_1, p. ehaf784.1884, 2025, doi: 10.1093/eurheartj/ehaf784.1884.

[68] T. Liu and D. Ai, "Roles of lipoxygenases in cardiovascular diseases," *J. Cardiovasc. Transl. Res.*, vol. 18, no. 3, pp. 599–610, 2025, doi: 10.1007/s12265-025-10605-2.

[69] M. Back, "Inhibitors of the 5-lipoxygenase pathway in atherosclerosis," *Curr. Vasc. Pharmacol.*, vol. 15, no. 27, pp. 3116–3132, 2009, doi: 10.2174/138161209789058020.